Mon. Not. R. Astron. Soc. **000**, 000–000 (0000) Printed 1 March 2017 (MN LATEX style file v2.2)

Slow Cooling in Low Metallicity Clouds: An Origin of Globular Cluster Bimodality?

Ricardo Fernandez[1] and Greg L. Bryan[1,2]
[1]*Department of Astronomy, Columbia University, 550 West 120th Street, New York, NY 10027, USA*
2*Center for Computational Astrophysics, Flatiron Institute, 162 Fifth Avenue, New York, NY 10010*

ABSTRACT

We explore the relative role of small-scale fragmentation and global collapse in low-metallicity clouds, pointing out that in such clouds the cooling time may be longer than free-free time, allowing the cloud to collapse before it can fragment. This, we argue, may help explain the formation of the low-metallicity component of globular clusters, since such dense stellar systems need a large amount of gas to be collected in a small region (without any star formation during the collapse). We carry out numerical simulation of low-metallicity Bonner-Ebert stable gas clouds, demonstrating that there exists a critical metallicity (between 0.001 and 0.01 $Z_{\odot}$) below which the cloud collapses globally without fragmentation. We also run simulations including a background radiative heating source, showing that this can also produce clouds that do not fragment, provided the metallicity is again below a critical value (which depends on the heating rate and is generally larger than the no-heating case).

Key words: globular clusters - methods:numerical

1 INTRODUCTION

Globular clusters (GCs), with typical masses of 10^5-10^6 $M_{\odot}$ are particularly interesting relics of star formation for a number of reasons: (1) the are very concentrated, with half-mass radii of a few parsecs, indicating that star formation occurred in a particularly dense environment; (2) the stars in a given GC generally have a very narrow spread in ages and metallicity, implying a single stellar population (although recent results have revealed a more nuanced situation here, as we will discuss briefly later), and (3) the metallicity distribution of GCs in external galaxies is generally bimodal (or at least very different from the metallicity distribution of stars in the galaxy as a whole), with a large number of low-metallicity GCs. Reviews of their properties include Brodie & Strader (2006), Renzini (2008, 2013), and see also Portegies Zwart, McMillan & Gieles (2010).

This bimodal, or possibly skewed metallicity distribution (e.g., Strader et al. 2003; Peng et al. 2006) is sometimes interpreted as indicating that there are two formation modes: one that produced low-metallicity, old systems and a second for the generally younger, higher-metallicity component. For instance, Ashman & Zepf (1992) suggested that metal-rich GCs are formed in gas rich mergers and metal-poor GCs are donated by progenitor spirals. However, their work did not incorporate a cosmological model, and their predictions of the number and color distribution of GCs in massive Es galaxies were not consistent, as pointed out by Forbes, Brodie & Grillmair (1997). Other models explored reionization for setting the bimodality (e.g., Santos 2003; Harris & Pudritz 1994).

Beasley et al. (2002) augmented this picture by incorporating a semi-analytical model of combined galaxy and GC formation in a cosmological context. In that work, each mode of GC formation was assigned a fixed efficiency relative to the field stars. However, to match observed values, the formation of metal-poor GCs had to be artificially truncated after $z = 5$. Recently, investigations have explored more empirical, hierarchical galaxy formation models in a cosmological setting. Muratov & Gnedin (2010) have modeled the formation of GCs using the assembly history from cosmological simulations combined with observed scaling relations. In their model bimodality naturally arises from the rate of galaxy mergers. Early mergers preferentially produce metal-poor GCs and a few late massive mergers can produce a significant number of metal-rich GCs. However their model produces metal-rich GCs that are too young, which is at odds with observation that some of metal-rich GCs are old as metal-poor GCs. In addition, their model is again semi-analytic and doesn't explicit deal with how star formation proceeds in low-metallicity, high-density gas.

Essentially none of the models discussed above attempt to model the detailed structure of star formation within globular clusters. In particular, it is not clear how to get a large amount of gas (10^6 $M_{\odot}$) into a very small region without star formation occurring during the collapse, which

would result in a wide spatial distribution of stars and perhaps even prevent the collapse.

As an aside, we note that, quite recently, observations have demonstrated that globular clusters are not a single stellar population, but may be composed of multiple generations showing enhanced He and specific abundance changes, particularly those associated with proton-capture processes (e.g., Norris et al. 1981; Kraft 1994; Gratton et al. 2001; Carretta et al. 2009). In addition, photometric data shows a splitting of the man sequence in many GCs Piotto (e.g., 2009); Anderson et al. (e.g., 2009); Milone et al. (e.g., 2010). This has been challenging to explain because, with a few possible exceptions, the Fe abundence distribution is generally very narrow (consistent with observational errors), indicating that supernova self-enrichment plays no role. A wide range of models have been proposed to explain these abundance irregularities, beginning with the possibility that AGB stars in the 4-8 $M_\odot$ mass range can produce the necessary elements through hot bottom burning (e.g., D'Ercole et al. 2010; Ventura et al. 2013). Other ideas include the existence of Fast Rotating Massive Stars (FRMS Krause et al. 2013), supermassive stars (Denissenkov & Hartwick 2014; Denissenkov et al. 2015), and massive interacting binaries de Mink et al. (e.g., 2009); Bastian et al. (e.g., 2013). All of these solutions are problematic for a number of reasons (e.g., Renzini 2015; Bastian, Cabrera-Ziri & Salaris 2015), including the mass budget required to generate the observed number of second generation stars. However, in this work, we will not explicitly explore this second generation, instead focusing on the problem of understanding star formation in low-metallicity gas.

2 BASIC IDEA

In this paper, we explore a simple idea: can the cooling properties of low-metallicity gas clouds themselves influence how star formation proceeds? High-metallicity (by which we mean approximately solar metallicity, or even lower – we will address this point more precisely below) gas cools rapidly, typically on a timescale shorter than the dynamical time, meaning that present day large gas clouds, with masses in the GC range, are typically "cold", with temperatures well below their virial temperatures and so rapid fragmentation is inevitable. This generally means that high-metallicity giant molecular clouds will rapidly produce stars before they are completely collapsed and feedback from those stars will result in a low star formation efficiency (REF). However, for a low enough metallicity, the gas may cool slowly so that the cloud will collapse coherently, not fragmenting until the central gas density is very high. These high densities promote rapid star formation resulting in high efficiency. In this way, paradoxically, inefficient cooling may result in more efficiency star formation. **Hoyle REF**

To further investigate this simple idea we have created one zone models of a cooling parcel of gas. In this scenario, the parameter space consists of density, temperature, and metallicity. Once the parameters are chosen the evolutionary timescales are computed: the quantity of interest is the ratio of the absolute value of cooling time to dynamical time $|t_{cool}|/t_{dyn}$. In our simple one zone model, cooling is computed using the publicly available GRACKLE chemistry library; details of implementation and functionality can be found in Bryan et al. (2014).

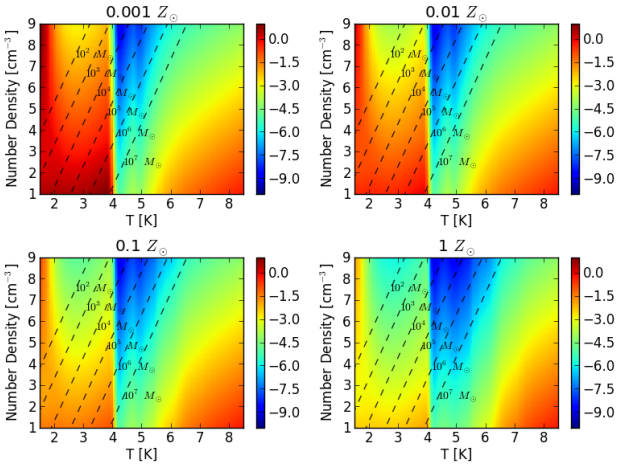

Figure 1. The ratio of cooling time to dynamical time for gas with a range of density, temperature and metallicity values, as labelled.

Figure 1 is a panel showing the ratio of $\log(|t_{cool}|/t_{dyn})$ for metallicity values $Z/Z_\odot = 10^{-3}, 10^{-2}, 10^{-1}, 1$. To begin, we focus on the lowest metallicity (upper-left) panel of Fig 1 – we see that there are two regions where cooling and dynamical time are comparable (shaded red). The first is in the temperature range $10^1 - 10^4$K (the sharp cutoff at 10^4K is due to efficient cooling from HI line emission), and the second is in the bottom right corner. It is the former region in which we are most interested because this area is where we expect to find gas clouds with values conducive for globular cluster formation. Over each heat map, we plot lines of density and temperature corresponding to constant Bonner-Ebert mass (see Section 3 for details on how this is computed). It is clear from the plot that, for gas clouds with masses typical of globular clusters, there are values in the region where cooling is relatively inefficient, allowing the gas to collapse coherently before it can cool and fragment. Further, as the metallicity increases this region becomes less pronounced and the gas becomes more efficient in cooling, which will allow the gas to cool and fragment before global collapse sets in.

This is all computed in the absence of any radiative background. In Figure 2, the one zone models are recalculated as previous except allowing for radiative heating. Although the radiative background is uncertain, we adopt the radiative background from Haardt & Madau (2012) at z =0 in order to show the kind of effect we expect. This does not change the high gas cooling rate, but it does affect the lower-temperature gas cooling time. In particular, we see that an equilibrium curve is present where heating and cooling are balanced. We no longer have the extended region where cooling and dynamical time scales are comparable but now are concentrated along the equilibrium curve. Furthermore, it should be expected that gas will naturally seek the equilibrium curve values. Therefore, for values above and below the curve there should be a migration to high density low temperature for values above and low density high temperature for values below. Moreover, when the the metallicity

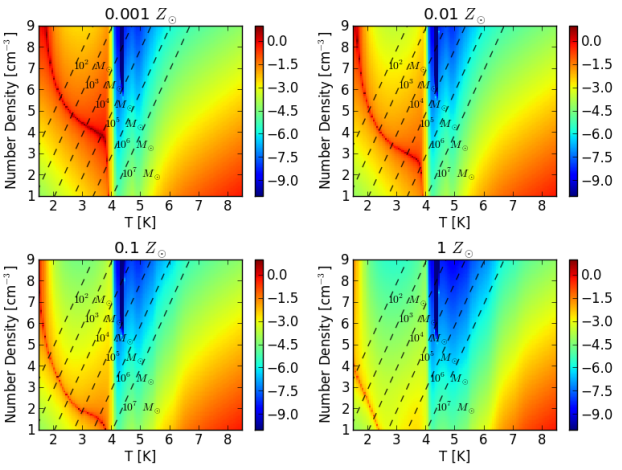

Figure 2. The ratio of cooling time to dynamical time for gas with a range of density, temperature and metallicity values, as labelled. This plot is similar to Figure 1, except that we include a radiative heating source as specified in Haardt & Madau (2012), at z =0.

increase the equilibrium curve shifts downward, decreasing the possibility of having globular cluster like conditions.

This is all determine by computing cooling and dynamical times for gas with a characteristic density and temperature, demonstrating that the idea of inefficient cooling may be appropriate for low-metallicity gas (or gas with a somewhat higher metallicity but stronger radiative background). We now turn to space- and time-dependent numerical simulations to explore this idea further. Ideally, we would carry out cosmological simulations that included the full range of dynamical processes relevant for star formation at high-redshift with low (but non-zero) metallicity. However, this is computational intractable, and therefore we instead investigate a simple, idealized set up. We expect that gas cloud collisions during mergers at high-redshift will result in the accumulation of gas in relatively dense knows. These clouds will rapidly cool to temperatures around 10^4 K. Therefore, we set up turbulently perturbed Bonner-Ebbert spheres with masses typical of globular clusters, and densities/metallicities motivated by Figure 1. In future work, we will explore more complicated dynamics, such as colliding flows; however, here we explore perhaps the most simple possible test of this idea.

3 NUMERICAL MODELS

3.1 Numerical Method

The simulations in this paper were performed with the publicly available Eulerian three-dimensional hydrodynamical adaptive mesh refinement Enzo code (Bryan et al. 2014). The domain box size of the simulation was 150 pc on a side with a top level root grid resolution of 128^3, and a maximum refinement level of 3, for a minimum cell size of 0.125 pc. Cell refinement was dictated by the gas mass such that a cell was refined whenever the its mass became larger than 0.1 $M_\odot$. In addition, we refined based on the Jeans length such that it was always refined by at least 4 cells (up until the maximum refinement is reached).

Our simulations included self gravity and radiative cooling using the GRACKLE library; details described in Bryan et al. (2014). The metal cooling (and heating) rates are computed using a non-equilibrium model for H, H^+, He, He^+, He^++ and e^- and a table computed from Cloudy for metal-line cooling (and heating), as described in Smith et al. (2016). When a radiative background is included, we use Haardt & Madau (2012) at z =0

3.2 Initial Conditions

Our initial conditions consist of a cloud in pressure equilibrium with an constant ambient density and temperature background. The internal structure of the cloud is modeled by a Bonner-Ebert sphere Bonnor (1956): a self-gravitating isothermal gas sphere in hydrostatic equilibrium embedded in a pressurized medium. To fully describe a Bonner-Ebert sphere, a mass M_{BE}, temperature T_{BE}, and an external pressure P_{ext} must be chosen. Following our assumptions outlined in Section 2, we chose $M_{BE} = 10^6$ $M_\odot$, $T_{BE} = 6000$ K, and $P_{ext} = 1.8 \times 10^5 \times k_B$, where k_B is the Boltzmann constant. This corresponds to a cloud on the point of gravitational collapse within nearly comparable cooling and collapse times, depending on the chosen metallicity (which we will vary).

Such a cloud may naturally arise during the early formation history ($z \sim 5$ to 10) of typical galactic halos [REF]. The virial temperatures of such progenitor halos are typically around $t_{\rm vir} \sim 10^{4-5}$ K, and the required densities of our cloud correspond to roughly an overdensity of 10^4 relative to the mean at that epoch. Therefore our required densities are modestly above typical halo properties and require only a modest amount of cooling. We note in addition that it is natural for the gas temperature to stall at temperatures just below 10^4 K for such low metallicity gas, as the above figures make clear. Finally, we do not discuss the fate of any dark matter in this scenario, but note that our clouds are most likely to form during the merger phase of such halos, when dynamics can lead to compression and so the clouds may well form away from the central dark matter peak.

In addition, we add turbulence to the cloud following a power spectrum of $v_k^2 \propto k^{-4}$ for the velocity field. We include only mode between $k_{\rm min} = 9$ and $k_{\rm max} = 19$ **(units?)** such that the input modes are well resolved and have wavelengths smaller than the cloud radius. We set the turbulent velocities such that rms velocity of the gas is 7.97 km/s. We use this initial conditions for essentially all of the runs analyzed in this paper.

Add table listing runs with Z, radiation strength.

4 RESULTS

We now carry out a set of simulations exploring the evolution of this cloud under a variety of conditions, with a particular emphasis on the impact of metallicity on their evolution. We begin, for simplicity, with models without any radiative background.

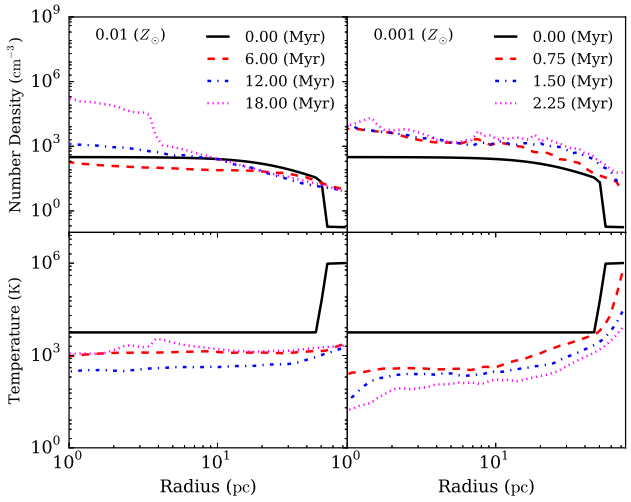

Figure 3. Cell mass weighted profiles for density (top panel) and temperature (bottom panel) as a function of radius at various output times, as shown, for runs with cooling, turbulence, and metallicity of $Z = 10^{-3} Z_\odot$ (left column) and $Z = 10^{-3} Z_\odot$ (right column).

4.1 No Heating Runs

4.1.1 $Z = 10^{-3} Z_\odot$

We start with a low metallicity gas – adopting $Z = 10^{-3} Z_\odot$ puts us well into the regime where the gas cooling time is longer than the gravitational collapse time (see the previous section). In the left panels of Figure 3, we show density and temperature profiles at a range of times during the collapse, stopping when high densities are reached and we can no longer accurately follow the evolution (the Jeans length criteria cannot be met even at our highest allowed refinement level). The cloud, which is initially stable (i.e. in pressure equilibrium), starts to evolve due to both the added turbulence and to gravity plus cooling. The free fall time of the cloud is $t_{ff} \approx 3$ Myr. However, the slow cooling time delays the immediate large scale collapse. This can be seen by the flat density profiles at times earlier than about 15 Myr. In fact, the cloud initially expands due to the added turbulence. The outer rim of the cloud moves outward, initially decreasing the density in the center. The expansion lasts for approximately 10 Myr, and during this time the temperature drops moderately (by about a factor of 2), mostly due to the expansion. By 18 Myr, the gravitational collapse sets in and a dense central core forms. The bottom left hand panel of Figure 3 shows the temperature profiles, with the temperature rising mildly during the recollapse, but not heating above about 1000 K due to radiative cooling.

More detail of this collapse can be seen in Figure 4, which shows the slices of density (left set of 6 panels) and temperature (right set of 6 panels) for this low metallicity run on the left side of each set of panels. We select the same times as in Figure 3 (6, 12 and 18 Myr after the initial time). Clearly the the turbulence drives substantial fluctuations in the density (and temperature), but the cloud does not fragment, undergoing global collapse. As expected from the one zone model, the cloud cannot efficiently cool before global gravitational collapse sets in.

4.1.2 $Z = 10^{-2} Z_\odot$

We repeat the previous run except we increase the metallicity to $Z = 10^{-2} Z_\odot$. The profiles are shown in the right-hand side of Figure 3 and the density/temperature slices on the right-hand side of the panels in Figure 4. In this case the evolution is very different. The gas can now cool efficiently, as evident particularly in the temperature profiles. The center of the gas cloud, up to radii of ≈ 10 pc, has cooled to ≈ 200 K in less than a million years. The added effect of the turbulence allows the cold gas to condense into dense pockets. This is seen clearly in the density and temperature slices, which show the formation of many dense, self-gravitating clumps. Hence, we see again that our numerical runs agree with our simple one zone models. Moreover, we find that there is a critical metallicity between $10^{-3} - 10^{-2} Z_\odot$ that separates the evolution of gas cloud into either global gravitational collapse or local fragmentation.

Note that the times shown in the profiles and slices differ between the two runs because we stop the calculation in both cases when dense gas clouds form and we are no longer able to follow the evolution even with our AMR run. In each run, at this point, star formation would rapidly occur and so we stop the calculation.

4.2 Runs with Photo-heating

4.2.1 $Z = 0.01$, *varying heating*

We next turn to simulations which include the impact of radiative heating, either from a metagalactic background or from nearby star formation (but assuming there is no direct physical impact on our cloud). We have carried out two additions simulations to explore this: the first has a radiative background typical of the Haardt & Madau (2012) metagalctic background at $z = 0$, as modeled with our cooling package GRACKLE (and ultimately Cloudy). This is a relatively mild heating source, but is sufficient to heat the low-temperature gas at low metallicity (see Figure 2 for the resulting cooling times). The second simulation adds an additional specific heating rate of 8.25×10^{-26} erg/s/g, as might arise from a photo-electric heating term arising from a nearby unattenuated UV source.

Figure 5 shows the radial density and temperature profiles for the two runs (left and right set of panels), and Figure 6 shows the density slices for the same set of times and heating rates, also for the two runs (left – low heating, right – higher heating). These plots demonstrate that a radiative heating source can substantially change the nature of the collapse, for a fixed metallicity ($Z = 0.01 Z_\odot$ in this case). Before discussing the results in more detail, we note that the later two times (t= 4.0 and 5.75 Myr) show a shock around the edges of the box due to the (artificial) periodic boundary conditions used. These shocks arise from a mild outflow driven by the expansion of the cloud – caused by the photo-heating – and do not affect the evolution in the central part of the cloud (the low density gas at the edges of the box is flowing faster than its sound speed).

In the mild heating case, collapse proceeds in a roughly

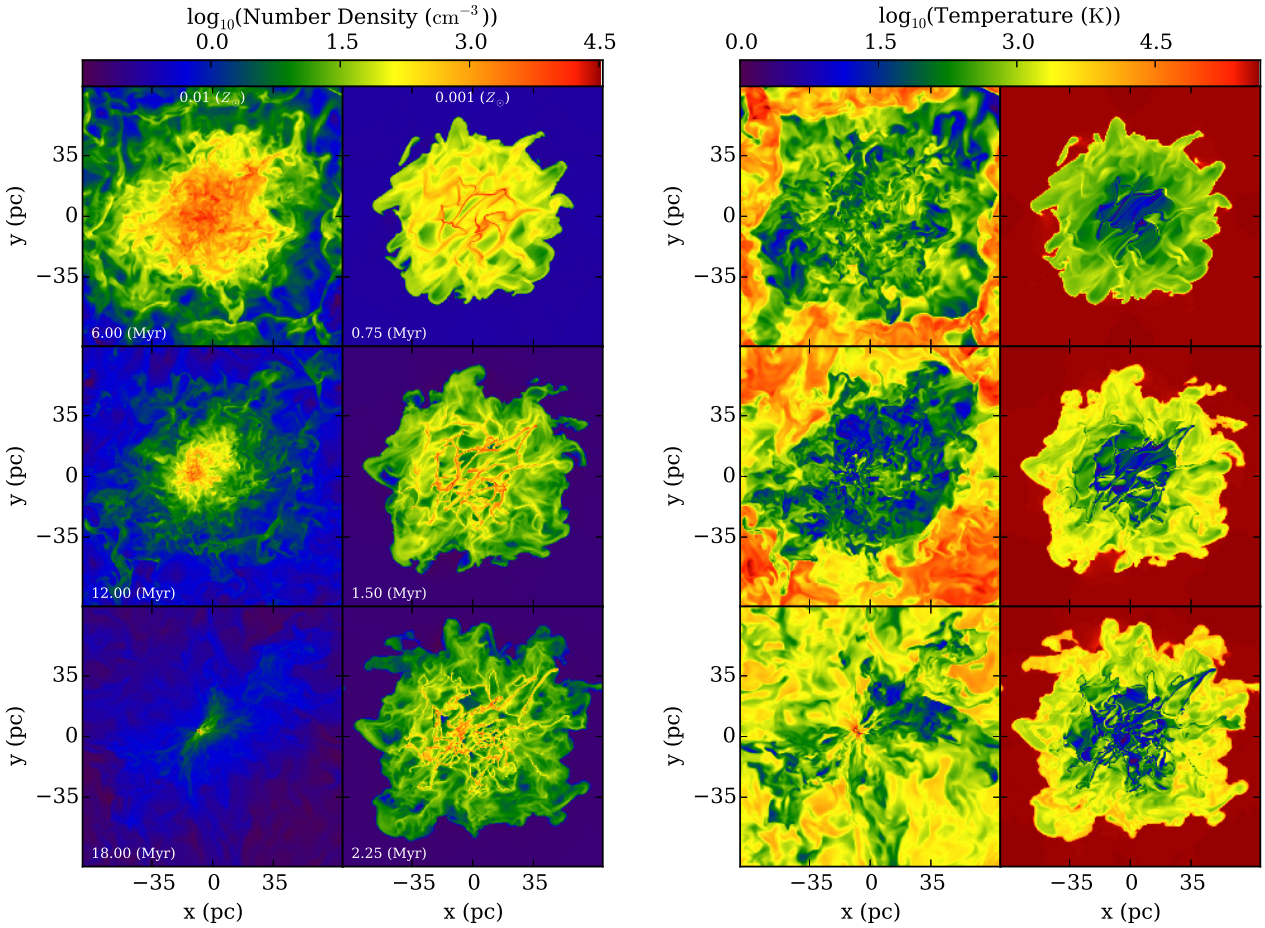

Figure 4. Density (left) and temperature (right) slices of the evolution of the sphere without radiative heating. Time evolution is from top to bottom and in each set of 6 panels, the left side is for the low metallicity ($Z = 10^{-3}Z_{\odot}$) run and the right-side side is for the higher (($Z = 10^{-3}Z_{\odot}$) run. The times are the same times as shown in the profiles in Figure 3.

similar fashion to the no-heating run, except that the temperature does not fall as quickly, particularly in the center. As the profiles and slices show, gas begins to fragment, but radiative heating prevents collapse to very high densities. Gas flows in to the center and fragmentation eventually sets in there, with densities climbing to large values in the central 5-10 pc. The cloud ends up with a central multi-phase core, with forming clumps, and a smooth outer envelope. The core is not quite as compact as for the $Z = 0.001$, no-radiation run, but compared to the $Z = 0.01$, no-radiation case, fragmentation only occurs in the central 5-10 pc.

The higher radiative heating case shows, despite only a relatively small increase in the heating rate, a substantially different evolution. Again, gas flows in and fragmentation begins in the central region, but this time the gas is unable to complete fragmentation, and the cloud ends up nearly entirely smooth with (almost) no star forming regions.

The reason behind this evolution is easier to understand through phase diagrams. In Figure 7, we show the density-temperature and pressure-temperature distributions of our two runs at the same times as in the previous plots. The gas starts at $t = 0$ (not shown) mostly in a small region in the right hand side of each diagram (with $T \sim 6000$ K and $P \sim 10^{-10}$ dyne cm^{-2}). In each case, the gas rapidly moves into thermal equilibrium and so follows the equilibrium density-temperature relation shown as a dotted line in the plots. The relation is particularly tight for the higher radiative heating run at late times, but is generally well-followed in all runs at all times. However, the larger difference is where the gas evolves to along this curve – at early times, in both cases, the gas is mostly in the warmer, lower-density phase. In the lower-heating run, some gas manages to cool and move into the upper left-region (where the Jeans mass decreases and star formation can commence), while in the higher heating run, essentially no gas moves in that direction.

The reason for this striking difference is made clear in the pressure-temperature distribution plot. Recall that the cloud begins in pressure equilibrium, with a small range of pressures. Therefore, the cloud has two constraints in this diagram: the equilibrium curve as shown, and a nearly constant pressure constraint, coming from pressure equilibrium in the cloud. This leads to multiple phases, since the equi-

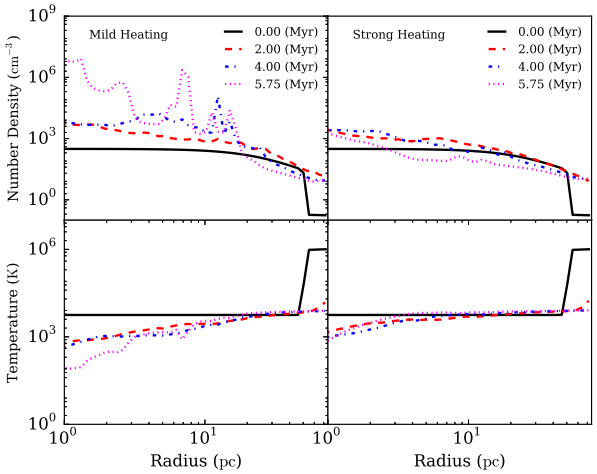

Figure 5. Cell mass weighted profiles for density (top panel) and temperature (bottom panel) as a function of radius at various output times, as shown, for runs with cooling, turbulence, and metallicity of $Z = 10^{-2} Z_{\odot}$ and mild heating (left column) and stronger heating (right column). See text for heating rates.

librium curve has a small region from 1000-5000 K where it is thermally unstable in the classic sense of REF. This produces two stable regions: one at low temperatures ($T \sim 1000$ K and below) and one at higher temperatures, close to 10^4 K.

In the low heating run, there is some gas in the lower temperature phase, and this gas would like to cool and move up the equilibrium curve to the left, but in order to do so, it must dynamically increase its pressure, which it eventually does through gravitational collapse (the amount of gas in this phase exceeds the Jeans mass, although it takes some time to collect together in the center of the cloud). In the higher heating simulation, there is essentially no gas in the lower phase, even though the extra heating is so small that it is difficult to see the small upward shift in the equilibrium curves in Figure 7. This small extra heating boosts the equilibrium pressure of the low-temperature stable phase above the cloud pressure and so it is inaccessible to the gas. The net result is a completely stable cloud, with no collapse or fragmentation.

Therefore we see that heating modifies the collapse by creating a multi-phase medium, and only the low temperature phase can gravitationally collapse. This is reminiscent of the situation in the interstellar medium at late times; however, here our cooling rates are much lower over all and so the densities are sufficiently high that the dynamical (gravitational) timescale of the overall ($\sim 10^6$ M$_{\odot}$) cloud becomes important.

In the discussion, we will develop a simple analytic model based on the insights described above and discuss how this model can be applied to physical conditions in order to create a more comprehensive picture for cloud collapse vs. fragmentation as a function of metallicity and radiative heating rate. However, first, we will explore one final model which features a more extreme case.

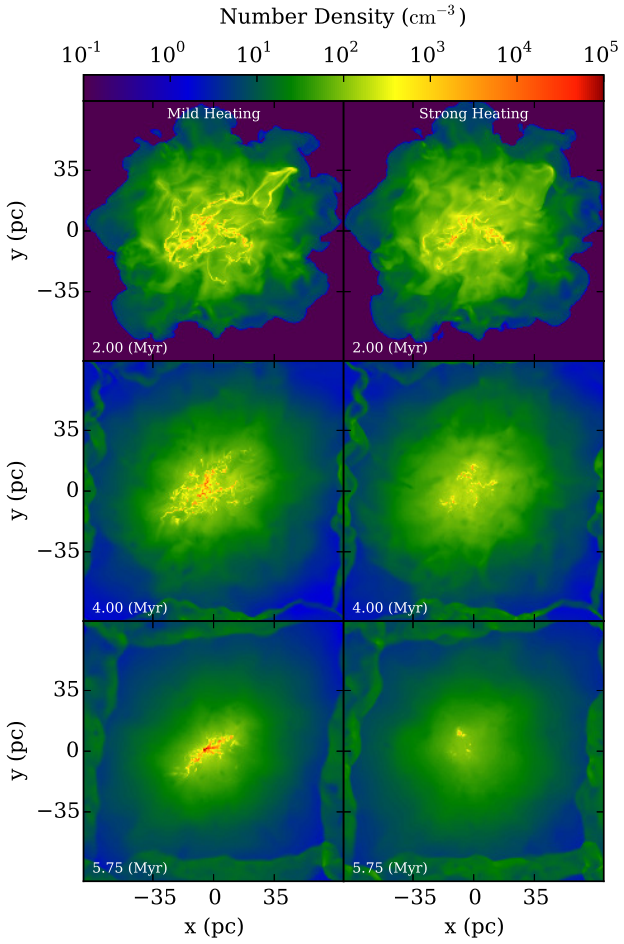

Figure 6. Density slices at three different output times (as in Figure 5) going from top to bottom for the two different heating, rates: mild heating (left column) and stronger heating (right column).

4.2.2 Higher mass, higher radiative collapse

Finally, to further explore the parameter space of cloud size and radiative background, we do one run with a five times larger mass, keeping the radius constant, which results in a significant increase in the density. Note that this means the cloud is no longer Bonner-Ebert stable and should not be gravitationally unstable to collapse even without any further cooling. Without any other change, the discussion above makes it clear that this cloud would simply fragment before collapsing since Figure 1 makes it clear that the cooling time to dynamical time ratio only decreases with increasing density. Note that we keep the metallicity at $Z = 0.01 Z_{\odot}$. The earlier discussion makes clear that increasing the radiative heating rate would enhance the stability, forcing the evolution of the gas along the density-temperature equilibrium curve. We test this by increasing the radiative heating rate by a factor of ten.

The result of this simulation is shown in Figure 8, where, unlike the previous images, we show the density and temperature projections. These show two things: first, as ex-

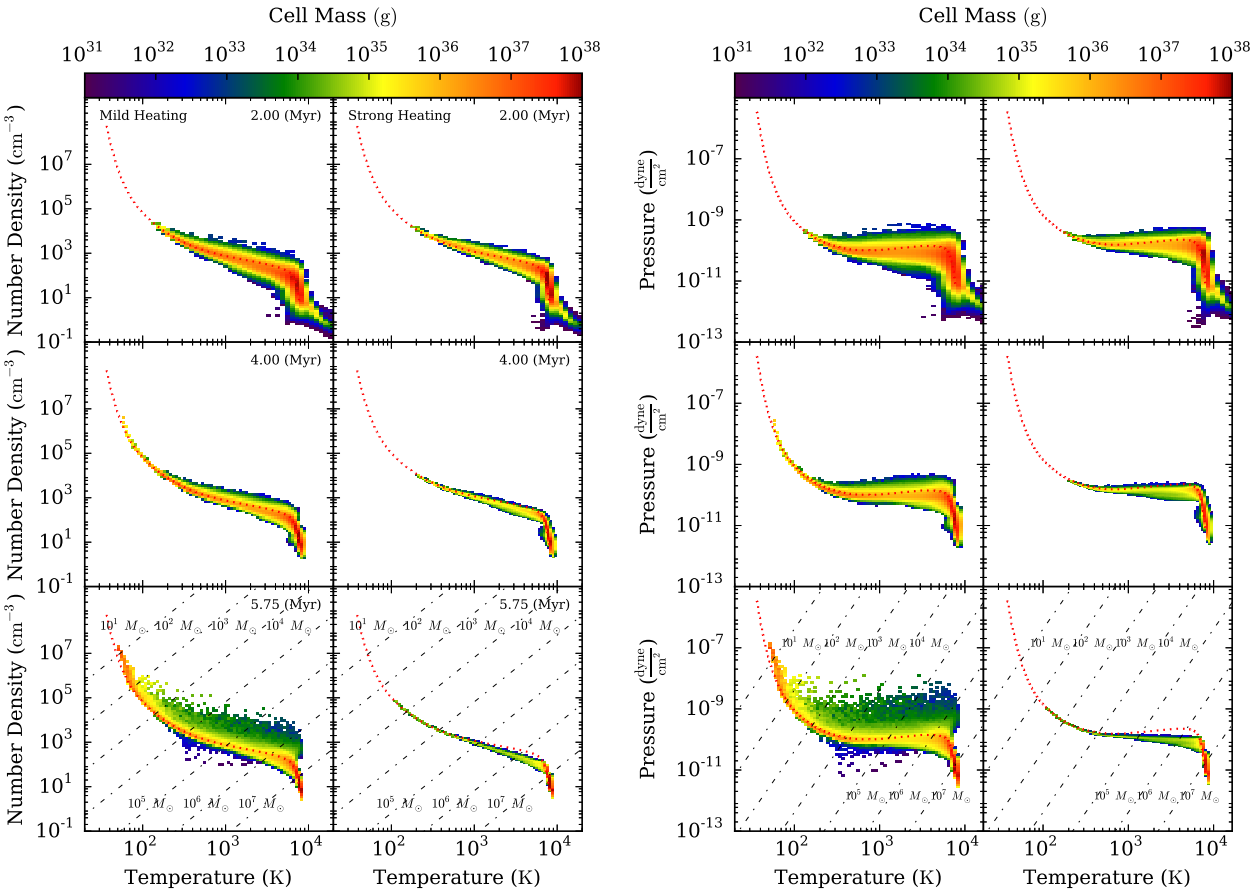

Figure 7. Phase plots showing, in the left set of panels, the density-temperature distribution and, in the right set of panels, the pressure-temperature of the gas in our two simulations with varying radiative heating rates. In each set of panels, time runs from top to bottom at the same time slices as in Figure 6, and within each set of 6 panels the left side is for the low-radiative heating run, while the right side is the higher heating simulation. The color coding indicates the amount of mass in each phase. In each plot, dotted lines show the equilibrium density-temperature relation, while dot-dashed lines in the bottom row provides lines of constant Jeans mass, as labelled.

pected, the fragmentation as been delayed due to the radiative heating, giving the cloud time to globally collapse before small-scale (turbulence driven) fragmentation occurs. Second, these projections emphasize the rich structure visible in the full three dimensional distribution, with clumps and filaments (these features were present in previous simulations but not as evident in the slices shown earlier). The density-temperature profiles (not shown) are consistent with the expected density-temperature equilibrium, and the overall profiles are also consistent with the earlier simulations which collapse globally before fragmenting. We do note, as we will discuss in more detail below, that this experiment is, in some sense pedagogical, as we have not attempted a self-consistent radiative transfer calculation.

5 DISCUSSION

Our numerical simulations paint a consistent picture: below a critical (low) metallicity, clouds can collapse globally before they fragment. Radiative heating acts to boost the critical metallicity. In the following sections, we first develop a simple analytic model which explains this result and shows how it scales with cloud mass, metallicity and heating rate. Then we briefly discuss the implications before listing the many shortcomings of this work, which is really intended more to be a proof of concept than a detailed physical model to be compared with observations.

5.1 Analytic Model

In Section 2, we outlined our basic idea, and in the previous section, demonstrated that, in principle, the effect can be important for specific parameter choices. Here, we try to create a *very* simple model of the key processes and to see how the critical cooling rate (or metallicity) scales with heating rate and cloud mass.

We begin by examining the models with radiative heating, as thermal balance results in a clear density-temperature relation. We will then extend this to the case without (radiative) heating. Assuming a simple power law cooling rate per particle $\Lambda(T) = \Lambda_0(Z/Z_0)(T/T_0)^{\alpha}$, (which

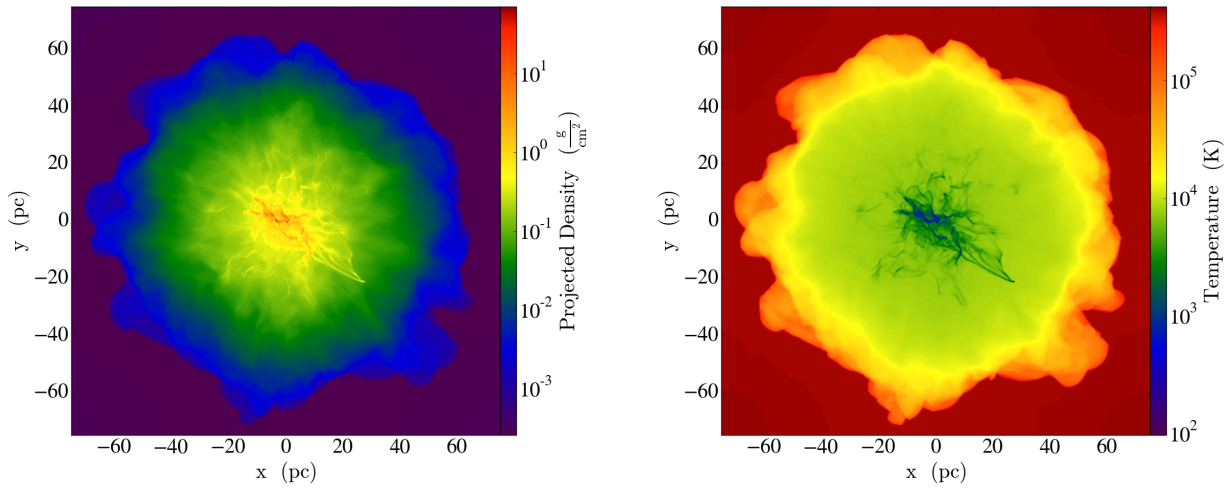

Figure 8. A projection of the surface density (left) and density-weighted temperature (right) for the large mass and high radiative heating rate simulation at t=1.5 Myr.

is a reasonably accurate below 10^4 K, for which $\alpha \approx 1$), thermal equilibrium can be written as,

$$\Lambda_0 \frac{Z}{Z_0} \left(\frac{T}{T_0}\right)^{\alpha} n^2 = \Gamma n \tag{1}$$

where Γ is the heating rate per particle. Conceptually fixing the temperature, this can be solved for density and used in the ideal gas equation to determine a pressure set by thermal equilibrium:

$$P_{\Gamma \rm eq} = \frac{\Gamma k Z_0 T_0^{\alpha}}{\Lambda_0 Z} T^{1-\alpha} \tag{2}$$

The right panel of Figure 7 (and associated discussion) shows that, before fragmentation sets in, the pressure is roughly constant, consistent with the above expression for $\alpha \approx 1$. This fails at both low and high temperatures, but is a good approximation for a wide range of temperatures (indeed the dotted line in these figures shows a better estimate of the equilibrium pressure).

The other constraint is global hydrostatic equilibrium, which is set by initial Bonner-Ebert critical initial conditions. There are a number of ways to parameterize this central pressure, but here we choose to do so in terms of the critical Bonner-Ebert pressure in the center:

$$P_{\rm cBE} = 19.9 \frac{\chi c_s^8}{G^3 M_{\rm BE}^2} \tag{3}$$

where we have allowed a possible overpressure value χ (note that $\chi = 1$ for all but the final run). In principle, we could rewrite c_s in terms of the temperature; however, we choose not to do so in order to remind ourselves that this is a global relation (note that we could also replace $P_{\rm cBE}$ with $\approx 10 P_{\rm ext}$, where $P_{\rm ext}$ is the external pressure).

The interpretation of these two pressures can be seen conceptually with reference to the right panels of Figure 7. For example, as the heating rate increases (or metallicity decreases), Eq. (2) indicates that the equilibrium pressure will increase, while the BE pressure is unchanged (this is equivalent to going from the left to right column). At a sufficiently high heating rate (the right column), or sufficiently low metallicity, the two curves cross only at high temperature, while the Jeans length is large and fragmentation is not allowed. For lower heating rate (left column) or sufficiently high metallicity, the thermal pressure allows a low-temperature solution and therefore a low Jeans length and so more rapid fragmentation. This argument is very similar to the classic multi-phase ISM, but with the additional scale imposed by the BE sphere and the Jeans length.

The above argument indicates that there is a critical point when these two pressure coincide. Equating our expressions these two pressures ($P_{\Gamma \rm eq} = P_{cBE}$) gives a critical metallicity:

$$Z_{\rm crit} = Z_0 \frac{k T_0^{\alpha} G^3}{19.9 \Lambda_0 \chi} \frac{T^{1-\alpha}}{c_s^8} \Gamma M_{\rm BE}^2 \tag{4}$$

and we can immediately read off the scaling with heating rate Γ linear, as expected and (Bonner-Ebert) cloud mass.

In addition to the case of thermal equilibrium between radiative heating and cooling, we can explore a model in which the heating is supplied by dissipation of turbulence. We assume this heating rate is given by $\sigma^3 \rho / L$, where σ is the turbulent velocity dispersion and L is the driving scale (here our largest turbulent scale so that $L = 2\pi/k_{\rm max}$). Note that this depends on the velocity dispersion, which decreases as the turbulence damps; however, we can set a balance at a given time. As before, we balance this heating with cooling, and can compute an effective equation of state.[1]

$$P_{\rm Teq} = \frac{\sigma^3 \mu k Z_0 T_0^{\alpha}}{L \Lambda_0 Z} T^{1-\alpha} \tag{5}$$

Following the same logic as before, equilibrium between these pressures can be used to find a critical metallicity:

[1] Note that this is *not* the turbulent pressure, but is instead the thermal pressure that arises from turbulent heating. A more complete description would add a turbulent pressure term here, but for simplicity, here we neglect that term which we expect to be subdominant.

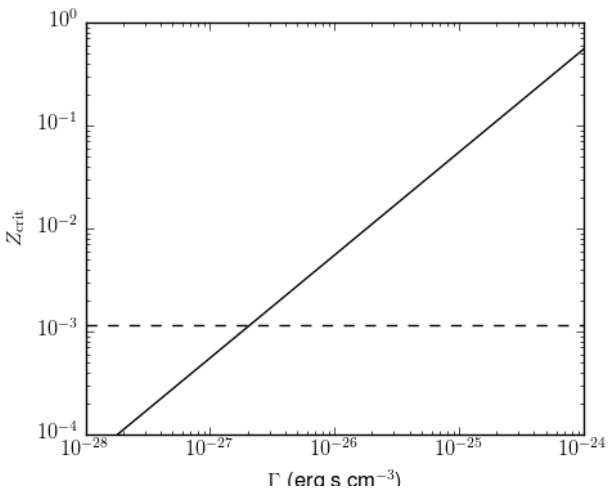

Figure 9. The critical metallicity as a function of radiative heating, indicating the dividing line between small-scale instabiity (above the line) and small-scale stability (below the line). The solid line shows the relation assuming heating is radiative, while the dotted line shows the relation for turbulent heating. See text for assumed values.

$$Z_{\rm crit} = Z_0 \frac{\sigma^3 \mu k T_0^\alpha G^3}{19.9 \Lambda_0 \chi} \frac{T^{1-\alpha}}{L c_s^8} M_{\rm BE}^2 \quad (6)$$

In Figure 9, we show these critical metallicity expressions. The solid line shows equation 4; above this line the cooling is sufficiently rapid that the thermal pressure allows fragmentation before global collapse, while below the line radiative heating prevents fragmentation. A similar argument holds for the turbulent-heated critical metallicity, although in this case the relation is σ (and hence time) dependent.

Note also the dependence on the BE mass (and sound speed) ...

5.2 Implications

As we have argued, the cooling efficiency may play an important role in the fragmentation of low-metallicity clouds. Paradoxically, low metallicity (or high radiative heating) may allow the gas in near primordial clouds to cool slowly enough that global gravitational collapse precedes local gravitational collapse (at least for a time). Our detailed simulations show that, in the absence of radiative heating, that critical metallicity is between 0.1% and 1% of solar metallicity. This is well below typical "blue" globular cluster metallicities, which are typically around a few percent. However, we have also shown that radiative heating can boost that critical metallicity to values similar to those observed.

Of course, our calculations are merely suggestive at this point, with many oversimplifications, as we will discuss in more detail in the next section. However, if we take this seriously, then it does provide an interesting "direct" explanation for the observed GC bi-modality. On the other hand, it begs the question about what creates higher-metallicity systems. In these cases, observations strongly suggest that rapid gas flows are required – for example the kind of colliding flows that we expect in galaxy mergers. In that case, the high velocities from the initial conditions (and presumably rapid cooling) permit gas to accumulate to high densities in a short period, circumventing the problem of small-scale fragmentation. In essence, rather than allowing the $\sim 10^6$ $M_\odot$cloud to collapse under its own gravity, the collapse time is boosted by the velocities of the larger (galaxy-massed) halo.

Therefore, a possible picture emerges of two modes of GC formation: one is a slow, low-metallicity mode in which the collapse timescale is the free-fall time of the proto-GC cloud; while the other is $\sim R/v_{\rm vir}$, where $v_{\rm vir} \sim 200$ km/s is the virial velocity of the parent halo.

5.3 Caveats

Here, we briefly remind readers of the many simplifications. As we have argued throughout, these calculations are intended to more suggestive explorations than realistic predictions.

First, the initial conditions are quite simplistic, with a Bonner-Ebert sphere and some imposed turbulence. We do not expect the results to strongly depend on the details of the turbulence; however we have not really discussed how such initial conditions might arise. One possibility is that colliding flows in low $v_{\rm vir}$ halos shock heat and cool down to 10^4 K (but not below), settling into the equilibrium configuration envisioned. More realistic (future) work would explore colliding flows or colliding clouds to better understand the transition between the fast and slow modes discussed above. Ideally, the initial conditions would be drawn from large-scale cosmological simulations which self-consistently model the gas motion within realistic dark-matter halos and the build-up of metals and external radiation fields (but cannot model the small-scale fragmentation modeled here).

More seriously, our radiative and chemical model is somewhat idealized. Although the GRACKLE cooling we adopt is based on Cloudy and so, radiative processes aside, quite accurate, our treatment of a uniformly constant radiative heating rate fails to take account the full complexity of more realistic treatments. Our uniform rate is best matched to a far-UV photo-electric heating source; however, the low metal content we assume implies a similarly low (or lower) dust content, reducing the efficiency of photoelectric heating. **Estimate background rate and require local SFR** Heating by an X-ray source would also provide uniform heating, but at the cost of additional ionization. In addition, local photoelectric heating would likely be accompanied by ionizing photons (although a large local column of neutral gas may slow the ionization front). Finally, we do not include H_2 cooling which may be important [GLOVER REF], although a Lyman-Werner background will help to photo-dissociate the molecule.

There are also a range of other physical processes that we do not include which may play a role in such systems, of which the absence of magnetic fields may be the most glaring. Finally, we explore the fragmentation of the clouds, but do not attempt to model the formation of individual stars, nor their feedback effects. Previous work that has examined the impact of feedback finds that in order to form bound clusters, the efficiency of star formation must be high [REFS], a result which helps to motivate our requirement that fragmentation must not occur until the gas density

is very high (so that fragmentation completes on a short timescale, before feedback can impact the cluster evolution).

6 SUMMARY

We have carried out simulations of low metallicity (but not primordial) gas clouds in order to better understand how such collapse proceeds. This is motivated in part by a suggestion that the low-metallicity (blue) population of globular clusters form preferentially from such low metallicity gas due to the possibility that the free-fall time is shorter than the cooling time in these clouds. In particular, we carried out a set of simulation of Bonner-Ebert stable clouds with densities of 10-100 cm^{-3}, radii of about 50 pc, and temperatures just below 10^4 K, with the following results.

(i) In the absence of radiative heating, there is a critical metallicity between $Z = 0.001$ $Z_\odot$ and $Z = 0.01$ $Z_\odot$, below which the cloud first collapses globally before fragmenting. For metallicities larger than this critical value, the opposite occurs, and the cloud first fragments. This is shown most clearly in Figure 4. The low metallicity runs result is a fragmenting cloud with properties (size and mass) reminiscent of present-day globular clusters; however, we note that this critical metallicity is lower than the typical values seen even in low-metallicity globular clusters.

(ii) Adding a radiative heating source (perhaps due to photo-electric heating although we have not included radiative transfer) changes the evolution. If establishes an equilibrium density-temperature curve and the gas ends up close to this curve in the simulations. Because of the temperature dependence of the radiative cooling at low temperatures, this gas is nearly at a constant pressure. We find that, if this thermal-equilibrium set pressure is lower than the hydrostatic pressure of the cloud, rapid fragmentation can occur; while if it is higher, then the cloud is largely stable. If the stable branch can then gradually collapse (either because the radiative heating rate declines or the cloud is driven globally gravitationally unstable due to cloud-cloud collisions or ongoing accretion), then high-density GC-like formation can occur.

(iii) For the radiative-heating case, we developed a simple analytical model based on the relative magnitude of the two pressures described above (the thermal-equilibrium pressure and the hydrostatic pressure), with the outcome either fragmentation or (local) stability. This lead again to the identification of a critical metallicity, but now one that depends on the radiative heating rate. This is shown in Figure 9.

Future steps would be to (i) improve the microphysical model with a more realistic heating and cooling model; (ii) better link the initial conditions to cosmological conditions in the high-redshift forming halos that host these gas clouds; and (iii) model the fragmentation to predict the initial mass function of such clouds, rather than a simple fragmention or no-fragmentation criterion.

ACKNOWLEDGMENTS

We acknowledge support from NSF grants AST-1312888 and AST-1615955, and NASA grant NNX15AB20G, as well as computational resources from NSF XSEDE, and Columbia University's Yeti cluster. Simulations were run on the Texas Advanced Computing Center Stampede supercomputer through allocation SMD-15-6514? and were performed using the publicly-available Enzo code (http://enzo-project.org) and analyzed with the yt package (Turk et al. 2011). Enzo is the product of a collaborative effort of many independent scientists from numerous institutions around the world. Their commitment to open science has helped make this work possible. The Flatiron Institute is supported by the Simons Foundation.

REFERENCES

Anderson J., Piotto G., King I. R., Bedin L. R., Guhathakurta P., 2009, ApJL, 697, L58
Ashman K. M., Zepf S. E., 1992, ApJ, 384, 50
Bastian N., Cabrera-Ziri I., Davies B., Larsen S. S., 2013, MNRAS, 436, 2852
Bastian N., Cabrera-Ziri I., Salaris M., 2015, MNRAS, 449, 3333
Bonnor W. B., 1956, MNRAS, 116, 351
Brodie J. P., Strader J., 2006, ARA&A, 44, 193
Bryan G. L. et al., 2014, ApJS, 211, 19
Carretta E., Bragaglia A., Gratton R., D'Orazi V., Lucatello S., 2009, A&A, 508, 695
de Mink S. E., Pols O. R., Langer N., Izzard R. G., 2009, A&A, 507, L1
Denissenkov P. A., Hartwick F. D. A., 2014, MNRAS, 437, L21
Denissenkov P. A., VandenBerg D. A., Hartwick F. D. A., Herwig F., Weiss A., Paxton B., 2015, MNRAS, 448, 3314
D'Ercole A., D'Antona F., Ventura P., Vesperini E., McMillan S. L. W., 2010, MNRAS, 407, 854
Forbes D. A., Brodie J. P., Grillmair C. J., 1997, AJ, 113, 1652
Gratton R. G. et al., 2001, A&A, 369, 87
Haardt F., Madau P., 2012, ApJ, 746, 125
Harris W. E., Pudritz R. E., 1994, ApJ, 429, 177
Kraft R. P., 1994, PASP, 106, 553
Krause M., Charbonnel C., Decressin T., Meynet G., Prantzos N., 2013, A&A, 552, A121
Milone A. P. et al., 2010, ApJ, 709, 1183
Muratov A. L., Gnedin O. Y., 2010, ApJ, 718, 1266
Norris J., Cottrell P. L., Freeman K. C., Da Costa G. S., 1981, ApJ, 244, 205
Peng E. W. et al., 2006, ApJ, 639, 95
Piotto G., 2009, in IAU Symposium, Vol. 258, The Ages of Stars, Mamajek E. E., Soderblom D. R., Wyse R. F. G., eds., pp. 233–244
Portegies Zwart S. F., McMillan S. L. W., Gieles M., 2010, ARA&A, 48, 431
Renzini A., 2008, MNRAS, 391, 354
Renzini A., 2013, Memorie della Societa Astronomica Italiana, 84, 162
Renzini A., 2015, in Astronomical Society of the Pacific Conference Series, Vol. 497, Why Galaxies Care about AGB Stars III: A Closer Look in Space and Time, Kerschbaum F., Wing R. F., Hron J., eds., p. 1
Santos M. R., 2003, in Extragalactic Globular Cluster Systems, Kissler-Patig M., ed., p. 348

Smith B. D. et al., 2016, ArXiv e-prints
Strader J., Brodie J. P., Schweizer F., Larsen S. S., Seitzer P., 2003, AJ, 125, 626
Ventura P., Di Criscienzo M., Carini R., D'Antona F., 2013, MNRAS, 431, 3642